Journal of Colloid and Interface Science 516 (2018) 371–378

Contents lists available at ScienceDirect

Journal of Colloid and Interface Science

journal homepage: www.elsevier.com/locate/jcis

Regular Article

Synthesis of nickel entities: From highly stable zerovalent nanoclusters to nanowires. Growth control and catalytic behavior

Ana S. Peinetti [a], Martín Mizrahi [b], Félix G. Requejo [b], David Buceta [c], M. Arturo López-Quintela [c], Graciela A. González [a], Fernando Battaglini [a,*]

[a] INQUIMAE (CONICET), Departamento de Química Inorgánica, Analítica y Química Física, Facultad de Ciencias Exactas y Naturales, Universidad de Buenos Aires, Ciudad Universitaria, Pabellón 2, C1428EHA Buenos Aires, Argentina
[b] Instituto de Investigaciones Fisicoquímicas Teóricas y Aplicadas, INIFTA (CONICET y Dto. Química, Fac. Cs Ex, UNLP), 1900 La Plata, Argentina
[c] Laboratory of Magnetism and Nanotechnology, Technological Research Institute, University of Santiago de Compostela, Santiago de Compostela E-15782, Spain

GRAPHICAL ABSTRACT

Synthesis of low atomicity Ni nanoclusters is carried out in 10 nm diameter mesoporous alumina allowing the production of zerovalent ligand-free Ni nanoclusters estimated in 13 atoms. The size and shape of the Nickel entities inside the pores can be controlled by the current density applied during the reduction process. The nanoclusters show a superior performance as catalysts for the reduction of methylene blue.

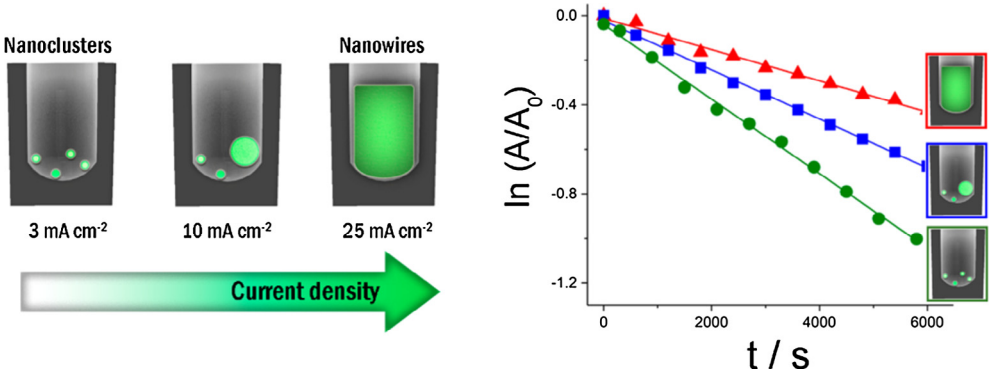

ARTICLE INFO

Article history:
Received 15 December 2017
Revised 22 January 2018
Accepted 23 January 2018

Keywords:
Nickel nanoclusters
Zero-valence nickel
Growth mechanism
Nickel nanowires
EXAFS and XANES characterization
Catalytic methylene blue reduction

ABSTRACT

Non-noble metal nanoclusters synthesis is receiving increased attention due to their unique catalytic properties and lower cost. Herein, the synthesis of ligand-free Ni nanoclusters with an average diameter of 0.7 nm corresponding to a structure of 13 atoms is presented; they exhibit a zero-valence state and a high stability toward oxidation and thermal treatment. The nanoclusters formation method consists in the electroreduction of nickel ions inside an ordered mesoporous alumina; also, by increasing the current density, other structures can be obtained reaching to nanowires of 10 nm diameter. A seed-mediated mechanism is proposed to explain the growth to nanowires inside these mesoporous cavities. The size dependence on the catalytic behavior of these entities is illustrated by studying the reduction of methylene blue where the nanoclusters show an outstanding performance.

* Corresponding author.
E-mail address: battagli@qi.fcen.uba.ar (F. Battaglini).

https://doi.org/10.1016/j.jcis.2018.01.083
0021-9797/

1. Introduction

Metal nanoclusters (NC) are a new class of materials which attract a great interest due to their new properties, related to their unique geometric and electronic structures [1–4]. The intrinsic features of these entities do not change monotonically; therefore, the controlled synthesis of these assemblies is highly relevant.

Although nanoclusters from noble metals are still the most studied systems [5–11], other elements such as Ni, Co, Fe and Cu are increasingly explored due to their interesting properties regarding magnetism and catalysis, their abundance and lower cost [12–15]. However, their synthesis showed to be an elusive subject, bringing new challenges due to their tendency to oxidize and the potential formation of unexpected intermediates or products [16]. Furthermore, if the element has magnetic properties (i.e., Ni, Fe, and Co), then the aggregation due to magnetic interactions between nanoparticles may occur and few examples can be found regarding their zerovalent nanoparticle synthesis.

In the case of Ni, organic-coated nickel nanoparticles (NiNPs) have been synthesized using microemulsion techniques [17], laser decomposition [18], or the reduction of metal ions in the presence of different organic ligands [19,20]. These ligands passivate the surface of the nanoparticles providing stability and yielding diameters of 5 nm or above. Crooks and coworkers [21] successfully synthesized NiNPs by reducing Ni ions inside dendrimers and obtained NPs with diameters smaller than 4 nm. Alonso et al. [12] could synthesize NiNPs smaller than 2 nm diameter using Li as reductant in an organic solvent. Synthetic approaches for preparing well defined Ni materials below the 2 nm size range are limited. Kumar et al. [22] synthetized Ni nanoclusters via a microplasma process, where the as-grown nanoclusters were deposited with an electrostatic precipitator onto carbon-coated Cu grids for a thoroughly characterization; however, no further ways of stabilization were shown. On the other hand, some groups were able to synthesize Ni nanoclusters capped with thiol derivatives ligands. Calderon et al. [16] carried out the synthesis of alkanethiol coated NiNPs obtaining a material comprised of some form of Ni(II)-alkanethiol polymer in coexistence with ultrasmall Ni clusters; while Joya et al. [23] were able to synthesize clusters capped with 2-phenylethanethiol in a well-established stoichiometry. Ni nanomaterials have shown to be excellent catalyst for a diverse group of reactions including hydrogen transfer [24], reduction of organic dyes from hazardous wastes [25], hydrogen production [26], water oxidation [23], among others. Additionally, the synthesis of Ni nanowires have attracted the interest in fields like catalysis [27] and magnetism [28,29].

In this work, we present the controlled synthesis of nickel entities from nanocluster to nanowires by using a hexagonally arranged porous alumina as a matrix. They are synthetized using a galvanostatic pulsed electrodeposition method, allowing the growth of 0.7 nm clusters when reduction current densities below 5 mA cm^{-2} are used. The nanoclusters are characterized by AFM and X-ray absorption spectroscopy (XAS) techniques presenting a high stability toward oxidation and thermal treatment. On the other hand, negligible effects in cluster size are observed when the alumina presents pore diameters between 5 and 18 nm, denoting the formation of a stable structure. Furthermore, by controlling the current of the electrodeposition process, the growth of these clusters toward greater entities is observed, allowing the synthesis of thin nanowires. The approach presented here provides the means for the synthesis of ligand-free highly stable zerovalent Ni nanoclusters with a narrow size distribution. Finally, the Ni growth process at different current densities is discussed and the performance of the Ni nanoclusters (NiNC) as catalyst is exemplified studying the reduction of methylene blue showing an outstanding efficiency.

2. Experimental

2.1. Materials and methods

All reagents were analytical grade. Water (18 MΩ cm^{-1}) was provided by a Millipore Simplicity equipment.

2.2. Nanoporous alumina (Al/Al_2O_3)

Working electrodes are prepared from aluminum 1145 (99.5%) with a surface of 6 mm^2. Surface pretreatment consisted in an electropolishing with ethanol:$HClO_4$ 5:1 at 18 V for 1 min. The cleaned surface was exposed to an acid electrolyte (15% H_2SO_4) at room temperature and a constant potential of 15 V was applied to the aluminum for 1 min, using a lead plate as counter electrode in front of the working electrode. Once the electrode was anodized, it was left 5 min in the acid environment. This step thinned the oxide barrier of the pores. The system is rinsed with water, dried with nitrogen current and ready for the next step. In this way a reproducible nanoporous structure is obtaining with the following characteristics: 11 ± 1 nm pore diameter, 1 μm depth and 35 nm interpore distance [30]. For pores sizes of 5 and 18 nm the applied anodization potentials were 10 and 25 V, respectively. SEM images of the alumina nanostructures are shown in Fig. S1 of the Electronic Supplementary Information.

2.3. Synthesis of Ni cluster (Al/Al_2O_3/NiNC) and other structures

Ni electrodeposition was carried out using a solution containing 100 g/L $NiSO_4{\cdot}6H_2O$, 45 g/L $NiCl_2{\cdot}6H_2O$ and 45 g/L H_3BO_3 at pH 4.5 as the electrolyte. Anodized aluminum and a gold plate were used as the working and counter electrodes, respectively. The different structures were obtained by electrodeposition performed at different current densities (J), ranging from −3 to −50 mA cm^{-2}. Three steps are involved in the electrodeposition process: (i) metal deposition at −J mA cm^{-2} for 8 ms; (ii) application of J mA cm^{-2} (2 ms) to decrease the capacitive oxide layer and interrupt the electric field at the interface where it is being deposited; (iii) no current is applied for 500 ms, to recover the ion concentration in the pores by diffusion from the solution. In total, 3000 pulses were performed, otherwise is noted.

2.4. Ni clusters dispersion

In order to obtain an aqueous dispersion of the clusters, Al/Al_2O_3/NiNC system was immersed in a 0.1 M NaOH solution during 30 min. Alumina is dissolved, yielding a solution with a high aluminate content.

2.5. Non contact-AFM measurements

XE-100 instrument (Park Systems Corporation) was used in non-contact mode. 20 μL of diluted Ni clusters dispersion in an aqueous solution was dropped onto a mica sheet, washed with Milli-Q water, and dried under nitrogen flow.

2.6. XAS techniques

Electronic and atomic structural parameters were determinate by X-ray absorption near edge structure (XANES) and extended X-ray absorption fine structure (EXAFS) experiments, respectively. Ni K-edge EXAFS and XANES spectra were measured at room temperature in fluorescence mode at the XAFS2 beamline at the Laboratorio Nacional de Luz Síncrotron (LNLS, Campinas, Brazil). An ionization chamber was used to detect the incident flux and a

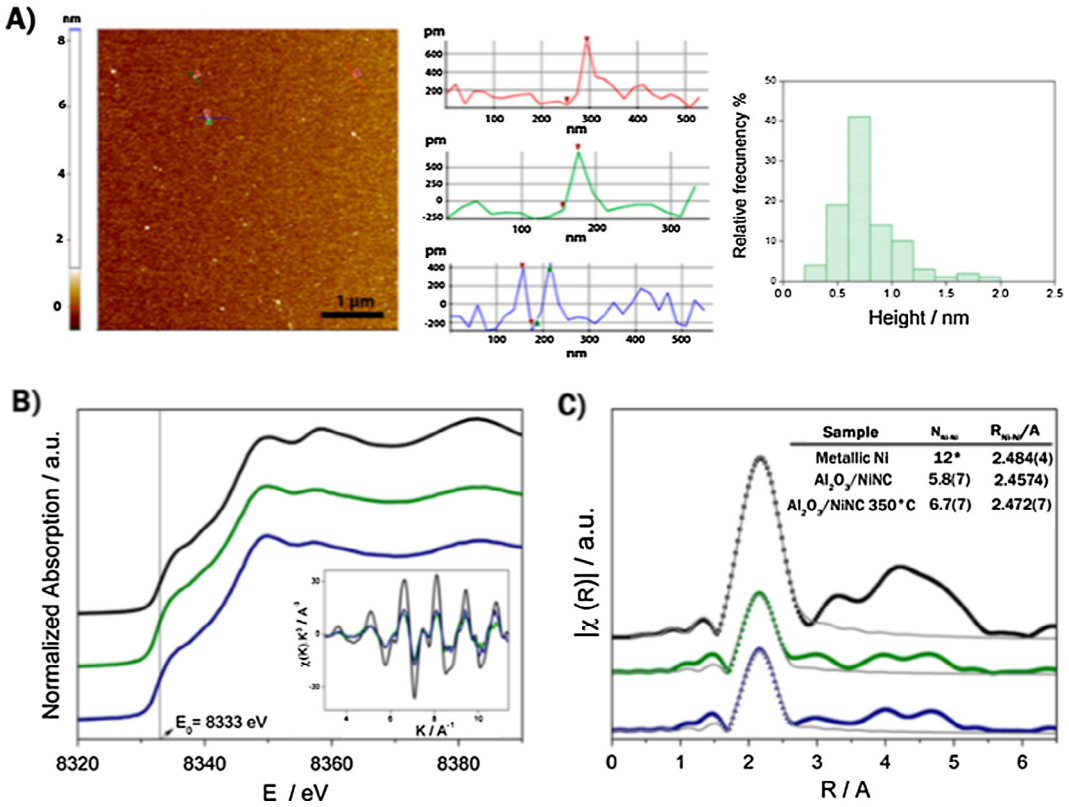

Fig. 1. (A) Left: NC-AFM topography images of Ni nanoclusters deposited on mica substrates. Center: section analysis of the lines of AFM images. Right: Histogram distributions heights. (B) Normalized XANES spectra at the Ni K-edge and EXAFS oscillation (inset) of bulk Ni reference (black line) and Al/Al_2O_3/NiNC at room temperature (green line) and at 350 °C (blue line). (C) Fourier transform of the EXAFS oscillation and the corresponded fittings (gray trace) for a bulk Ni reference (black) and the Al/Al_2O_3/NiNC sample at room temperature (green) and at 350 °C (blue). The Table in the inset summarized the average coordination number (N_{Ni-Ni}) and average interatomic distance (R_{Ni-Ni}) obtained from the fitting. Ni nanoclusters were grown at a current density of −3 mA cm^{-2} in a nanoporous alumina of 11 nm diameter. (For interpretation of the references to color in this figure legend, the reader is referred to the web version of this article.)

15-element germanium solid state detector was used to sense the fluorescence signal from the sample. Data were processed using ATHENA with the AUTOBK background removal algorithm [31]. The spectra were calibrated in energy using a foil of metallic nickel as reference. The EXAFS oscillations χ(k) were extracted from the experimental data with standard procedures using the Athena program. The k^3 weighted χ(k) data, to enhance the oscillations at higher k, were Fourier transformed. The Fourier transformation was calculated using the Hanning filtering function. EXAFS modeling was carried out using the ARTEMIS program which is part of the IFFEFIT package [31]. All measurements were performed without dissolving the alumina matrix.

2.7. Catalytic reduction of methylene blue

The catalytic reduction reaction of methylene blue (MB) was performed in an aqueous solution inside a quartz cuvette. Methylene blue (MB) solution and hydrazine hydrate solution were mixed and HCl was added to adjust the pH to 8.5. Immediately 24 mm^2 of the Al/Al_2O_3/NiNC were exposed to 0.7 mL of the solution containing 0.06 M hydrazine and 3.3×10^{-5} M MB, previously deoxygenated with N_2. The cuvette was immediately placed in the sample holder and the progress was monitored by recording the absorbance with a UV–Vis spectrophotometer at room temperature. Then, for catalytic studies, the changes in absorption at 665 nm with respect to time were measured. Control experiments were carried out using Al/Al_2O_3 where the electrodeposition step was not carried out. The amount of Ni in the aluminum samples were determined by inductively coupled plasma mass spectrometry (ICP-MS) (3iA Institute, University of San Martin, Argentina). The experiments were collected in duplicated and a value of 2.4 ± 0.4 μg of Ni in 24 mm^2 aluminum sample was obtained when a current of 3 mA cm^{-2} is applied.

3. Results and discussion

3.1. Ni nanocluster: Synthesis and characterization

A hexagonally ordered porous alumina with a structure of 11 nm pore diameter, 35 nm interpore distance and 1 μm depth was generated at the top of an aluminum rod. This structure was used as template for the synthesis of Ni nanoclusters. Nickel was electrodeposited from a 0.57 M Ni(II) solution at pH 4.5 using galvanostatic pulses involving three steps: first, metal deposition at −3 mA cm^{-2} to reduce the nickel ions; then, the application of 3 mA cm^{-2} for a shorter time to decrease the capacitive oxide layer; and, finally, no current is applied to recover the ion concentration in the pores (see Experimental Section for details). After 3000 cycles, no changes were observed in the appearance of the aluminum in contrast to previous works, where the deposition of nickel into alumina yields a colored product [32].

In order to determine the presence of possible formations of Ni inside the pores, the alumina was dissolved in sodium hydroxide to obtain a suspension of the entities. The suspension was investigated by atomic force microscopy (AFM) drop coating a mica substrate. This technique has atomic resolution along the vertical axis. AFM topography image and vertical section profiles of different clusters are presented in Fig. 1A. AFM results show the presence

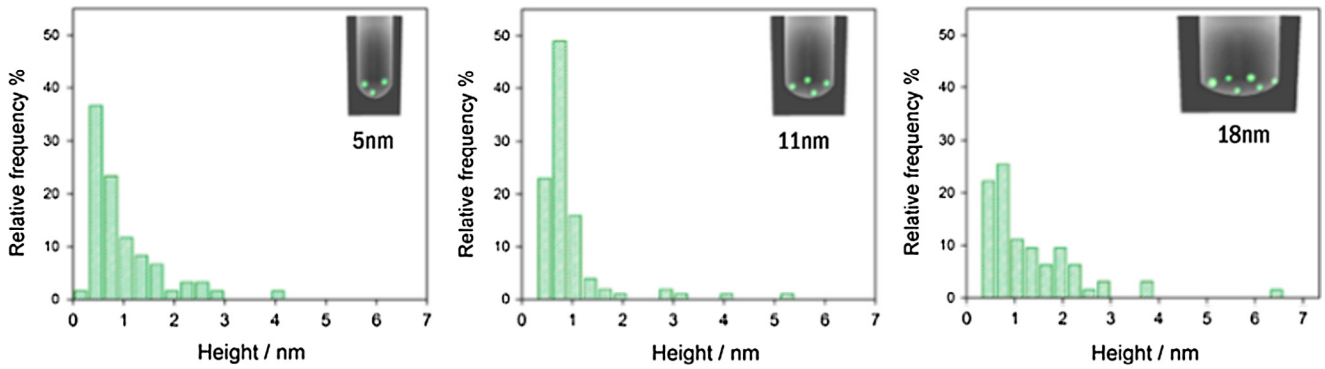

Fig. 2. Histogram distributions heights (n = 100) obtained from AFM images for Ni clusters samples produced at −3 mA cm^{-2} inside nanoporous alumina of 5, 11 and 18 nm pore diameter.

of clusters with an average height of 0.7 ± 0.1 nm (n = 100); the narrow distribution, confirms the formation of symmetrical particles with a sub-nanometric size.

The formation of nanoclusters inside the porous structure was studied *in situ* by XANES and EXAFS techniques. XANES spectra can be considered as a sensible fingerprint, which allows a direct comparison between spectra of samples and standard compounds, where their different features give information about the oxidation state and local atomic structure. Fig. 1B shows XANES spectra at the Ni K-edge of the Al/Al_2O_3/NiNC sample (green line) [1]and a metallic Ni reference (black line). These results indicate that the nickel electrogenerated in the nanoporous alumina is in its zerovalent form. It is important to mention that this measurement was carried out one month after the synthesis and they were in contact with air during this period. This remarkable resistance to oxidation can be attributed to the change from a metal conductor behavior to a molecular like behavior, where a band gap between the HOMO and LUMO appears [33].

EXAFS technique was employed to establish the nanoclusters structural characteristics *in situ*. It provides information about the average coordination number, type and distance between neighboring Ni atoms without altering the geometry of the sample. EXAFS oscillations at the Ni K-edge for an Al/Al_2O_3/NiNC sample and a bulk Ni reference are shown in Fig. 1B (inset). In both cases, the oscillation is similar, confirming that Ni clusters are in similar atomic local structure configuration than in bulk Ni. Also, the oscillation in the case of Ni clusters is attenuated respect to the reference bulk sample, as it is expected when the size is reducing.

The corresponding k^3-weighted Fourier Transform (FT) without phase correction of the EXAFS data and its fitted to the theoretical scattering formulas can be observed in Fig. 1C. The FT of the EXAFS spectrum at the Ni K-edge of Al/Al_2O_3/NiNC sample (green dots) was fitted using only a Ni-Ni shell, and no evidence of a Ni-O pair was found. An important decrease in the average coordination number (N_{Ni-Ni} = 5.8 ± 0.7) respect to the bulk nickel (N_{Ni-Ni} = 12) is observed (black dots), indicating that only a coordination shell around the Ni absorber atoms is present, being most of the atoms located at the surface. Then, this decrease in the average coordination number can be explained in terms of the drastic decrease in the particle size. Assuming spherical clusters, estimates of the particle average size can be made from a correlation with the average coordination number N_{Ni-Ni}. The average diameter obtained is (0.7 ± 0.1) nm, in good agreement with the average height found by AFM. Considering the average coordination number and average interatomic distance with their respective uncertainties (Fig. 1C, inset), an atomicity of 13 ± 3 can be proposed based on the calculations reported for these parameters [34,35]. A similar estimation can be derived using the diameters for Ni clusters of different atomicity recently reported [22].

These nanoclusters also present a high stability to thermal treatments. A XAS spectrum was taken after the sample was heated to 350 °C for 2 h under an air atmosphere to observe the electronic and structural changes could produce the heat treatment. Fig. 1B (blue line) shows the XANES spectrum of the sample heated to 350 °C; where practically no changes are observed after thermal treatment, indicating that the Ni remains in the zerovalent state. Further, Fourier transform (Fig. 1C (blue line)) of the sample after the thermal treatment presents a first sphere of coordination with a distance and amplitude similar to that found before the heating process. Sample fit shows that the average coordination number obtained is slightly higher than the one found in this sample before the thermal treatment; this could indicate that some clusters have begun to coalesce due to the thermal energy.

3.2. Growth mechanism: from Ni clusters to nanowires

To further elucidate the mechanisms of the cluster growth we analyze the influence of different parameters. Alumina with different pore diameters (5, 11 and 18 nm) were tested; for the smallest diameter, the nanocluster height distribution obtained by AFM is the same, while for the biggest, a slight increase in the cluster height distribution is observed (Fig. 2). The narrow size distribution at pores of 5 and 11 nm can be considered a direct consequence of the template-based synthesis [21]. However, the fact that even in 18 nm pores the main population corresponds to clusters of 0.7 nm height is indicative that we are in the presence of a stable superatom structure [36].

It is important to notice that increasing the current applied from −3 to −5 mA cm^{-2} new nucleation centers can be formed, without an appreciable change in the size of clusters (Fig. 3). In this sense, we can conclude that cathodic current densities below 5 mA cm^{-2} allow the synthesis of clusters with a well-defined structure. Increasing the current electrodeposition to −10 mA cm^{-2}, the presence of Ni nanoparticles begins to be observed. AFM analysis of the Ni structures formed in this condition still shows an important presence of clusters of less than 1 nm together with the nanoparticles (Fig. 3, right). The simultaneous presence of the two different atomic entities suggests that at higher currents the number of clusters in the same pore increases facilitating the formation of larger particles, probably due to the partial sintering of the clusters in the confined pore, yielding a bimodal size distribution. Also, the ICP-MS analysis shows that in this case the amount of Ni in the pores

[1] Please note that Figs. 1, 4, 7 will appear in B/W in print and color in the web version. Based on this, please approve the footnote 1 which explains this.

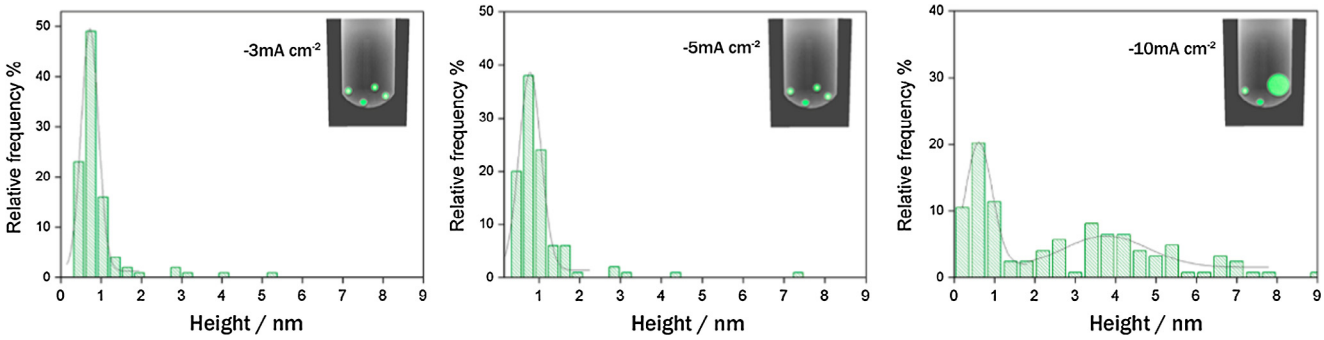

Fig. 3. Histogram of distributions heights obtained from AFM images for three Ni samples produced at different electrodeposition current densities.

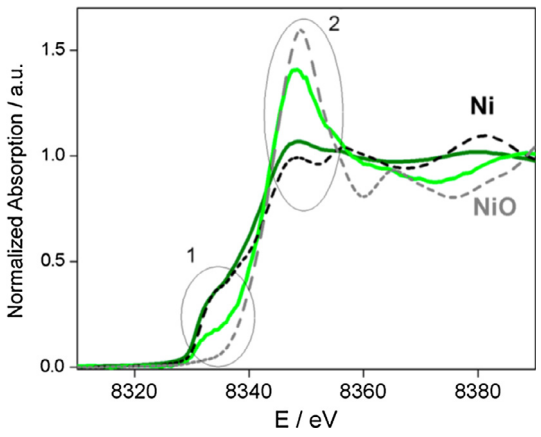

Fig. 4. Normalized XANES spectra at the Ni K-edge of Al/Al_2O_3/NiNC produced at -3 mA cm^{-2} (dark green) and -10 mA cm^{-2} (light green). A Ni reference (dashed black line) and a NiO reference (dashed gray line) are also plotted. Regions 1 and 2 show the two areas that allow distinguishing the Ni oxidation state. (For interpretation of the references to color in this figure legend, the reader is referred to the web version of this article.)

is 4 times greater than the one obtained when -3 mA cm^{-2} is applied.

In the presence of these larger nanoparticles, the XANES spectra show a strong contribution of NiO as it is shown in Fig. 4, indicating the oxidation of the nanoparticles. It can be observed that the patterns for the oxidized and elemental species are different; two features are useful to discern between an elemental Ni sample and an oxidized one. In the region close to 8330 eV (area 1 in Fig. 4), Ni(0) presents a shoulder, that it is not observed once the element is oxidized. On the other hand, the rising absorption edge leads to a sharp intense peak referred as "white line" (area 2 in Fig. 4), which is proportional to the oxidation state of the absorbing element. In the figure, the spectra for Ni samples obtained by applying -3 and -10 mA cm^{-2} (dark and light green lines, respectively) are plotted together with Ni and NiO spectra as references (black and gray dashed lines, respectively). It can be noted that the sample synthesized at -3 mA cm^{-2} fits with the Ni(0) spectrum in the critical areas, while the one produced at -10 mA cm^{-2} is intermediate between the two cases. This result is in agreement with the AFM experiments where two types of entities are present at -10 mA cm^{-2}, one with an average size below 1 nm, in accordance to the Ni(0) clusters observed for the -3 mA cm^{-2} case; while the other one corresponds to Ni nanoparticles, which, due to their size and metallic behavior, may be oxidized. From the linear combination of the two reference spectra an estimation of the degree of oxidation can be obtained, yielding a ratio of 70% oxide and 30% elemental Ni.

Finally, if a current density of -25 mA cm^{-2} is applied, Ni nanowires can be synthesized (Fig. 5), in accordance with previous results published by Goselle and coworkers for Ni in nanoporous alumina with wider diameters [32,37]. The nanowire height can be controlled by the number of pulses or the current density applied. The height of the nanowires was determined by SEM using a QBSE detector, which allows distinguishing elements due to their different atomic weights, therefore the presence of Ni in the porous alumina is enhanced. As an example, Fig. 5 (left) shows the nanowires formed when 3000 pulses and -50 mA cm^{-2} are applied. Also, the length can be increased applying more pulses (Fig. 5, right). Therefore, the growth process is guided by the porous size (diameter) and by the charge passed (length), leading to nanowires of 10 nm diameter with a narrow height distribution.

In order to understand the first steps of the growth mechanism, we explored the features of the Ni entities after a short number of

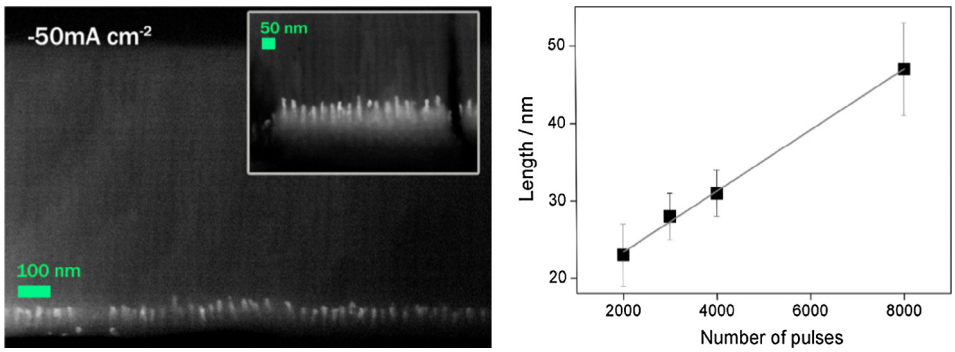

Fig. 5. Left: SEM image of the Ni nanowires. Ni electrodeposition was carried out at -50 mA cm^{-2} and 3000 pulses were applied. Right: Ni nanowire length as a function of pulse number applied. The electrodeposition is carried out at -25 mA cm^{-2}.

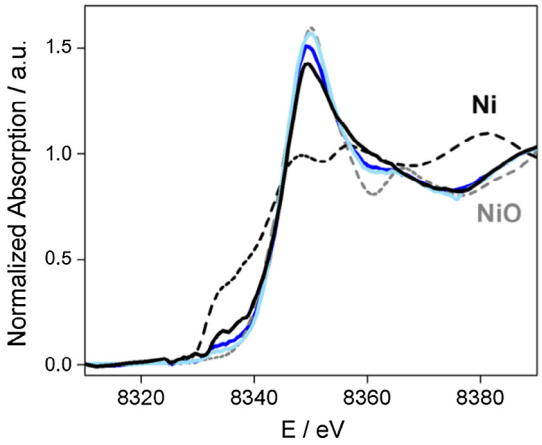

Fig. 6. Normalized XANES spectra at the Ni K-edge of Al/Al_2O_3/NiNC produced at -25 mA cm^{-2} applying 5 pulses (black), 50 pulses (blue) and 100 pulses (light blue). Ni and NiO references are plotted as in Fig. 4. (For interpretation of the references to color in this figure legend, the reader is referred to the web version of this article.)

pulses (5, 50 and 100) using -25 mA cm^{-2}. Fig. 6 shows the XANES spectra at the Ni K-edge for the nanoparticles formed in these conditions. From the beginning (5 pulses, black trace), it can be observed that the particles are mostly in the oxidized form, suggesting that they are mainly as nanoparticles. However, also a contribution of elemental Ni is observed; therefore, the presence of nanoclusters cannot be ruled out, following the same behavior that the one observed for NP grown at -10 mA cm^{-2}. As the number of pulses increases, the shape of the spectrum gets closer to the NiO, confirming the formation of a bulk-like structure. Overall, our results are compatible with the presence of clusters in this first steps of electrodeposition coexisting with oxidized nanoparticles.

The coexistence of the small clusters and the greater nanoparticles may explain the formation of the Ni nanowires. To date, two mechanisms have been proposed for the growth of nanowires. One involves the aggregation of nanoparticles [38,39] and the other one is a seed-mediated mechanism [40–42]. The last one involves the formation of nanowires by the catalytic reduction of metal ions on seed nanoparticles. This catalytic process is proposed to be induced by metallic nanoclusters. [43,44] Our results support the seed-mediated mechanism to explain the growth process since the coexistence of both types of particles is observed in the initial pulses of the electroreduction process. To further test this hypothesis, gold nanoparticles were synthesized in the same conditions than Ni. The characterization of these small nanoparticles and the dependence of its size with the synthesis parameters are shown in the Electronic Supplementary Material (Table S1). In the case of Au, where no evidence of nanoclusters is observed, the nanoparticles cannot growth to form nanowires, supporting the cluster-catalyzed growth mechanism.

3.3. Catalytic performance

The effect of the size of these Ni entities on the catalytic performance was studied by measuring the catalytic activity of a model reaction, the reduction of methylene blue (MB) by hydrazine.

The kinetics of MB reduction with hydrazine can be monitored by UV–vis spectroscopy, following the changes in the maximum absorbance wavelength (λ_{max} = 665 nm) of MB. As the concentration of reductant was much larger than the MB dye, the reaction could be considered as a pseudo-first-order reaction respect to MB. The effect of the structure in the reduction kinetics can be observed in Fig. 7 (top) where the reduction of MB with hydrazine

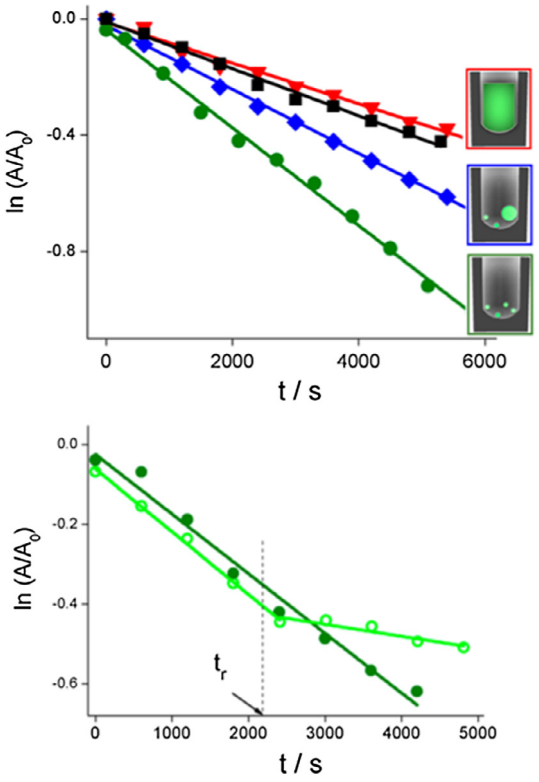

Fig. 7. (Top) Pseudo-first order plot of methylene blue reduction using different Ni structures generated at: -3 mA cm^{-2} (green circles), -10 mA cm^{-2} (blue diamonds) and -25 mA cm^{-2} (red triangles). Al/Al_2O_3 (black rectangles) is presented as control experiment. Absorbance was followed at 665 nm. (Bottom) Effect of removing (light green, open circles) or maintaining (dark green, closed circles) the clusters support after t_r. In both cases the reaction is carried out using Al/Al_2O_3/NiNC (-3 mA cm^{-2}) as catalyst. (For interpretation of the references to color in this figure legend, the reader is referred to the web version of this article.)

was carried out using Ni nanostructures synthesized at different current densities as catalysts.

When clusters are present the fastest catalytic activity for MB reduction (green dots) is obtained, demonstrating that this type of particles is responsible for the catalytic reduction. If the catalytic system is removed from the solution (Fig. 7, bottom, open green circles), the slope immediately changes and the pseudo-first order rate constant equals to the blank sample. This observation shows the high stability of the clusters inside the alumina and the advantage of using a heterogeneous catalyst that can be easily removed avoiding further purification steps. These results highlight the relevance of controlling the size Ni entity in catalytic processes.

Once taken into account hydrazine and Ni clusters concentrations, a rate constant value of 7×10^2 s^{-1} M^{-2} is obtained for the reduction of MB, comparable to the one reported for Cu_{13} clusters (9×10^2 $s^{-1}M^{-2}$) [45], that was up to now the hallmark of metallic particles catalytic activity.

4. Conclusions

Here we show for the first time that the pulsed electrodeposition of nickel confined in a porous alumina matrix successfully generates Ni nanoclusters. These clusters are ligand-free; present a zerovalent oxidation state and a 0.7 nm diameter corresponding to 13 atoms. The procedure is very robust since nanoclusters are obtained exclusively even at different pores sizes (5, 11 and 18 nm) and different current densities (-3 and -5 mA cm^{-2}). The high stability of the obtained clusters can be explained in terms

of the formation of superatoms where orbitals are created with a symmetry similar to atomic orbitals but delocalized throughout the entire cluster [46]. This delocalization confers the system a molecular-like behavior and stability, evidenced by its inertness toward oxidation and thermal treatment.

The synthesis of distinct Ni nanostructures at different conditions provide guidelines to postulate a mechanism regarding the growth of nanowires in confined systems. The experiments carried out at higher current densities show the formation of Ni clusters in its early stages, suggesting that the generation of greater structures only occurs when the nanoclusters are present. The coexistence of the small clusters and the greater nanoparticles explains the formation of the Ni nanowires, in accordance with seed-mediated model proposed for the growth of nanowires [41,42,44,47].

Finally, the clusters presented here show similar catalytic properties compared to copper clusters of similar size. At the best of our knowledge, this is the first report demonstrating the outstanding catalytic properties of ligand-free Ni nanocluster. On the other hand, the very thin diameter of the Ni nanowires obtained here (10 nm diameter) may give rise to unique physical properties [48] and represents an interesting starting point for further studies.

Acknowledgements

This work was partially supported by the following grants: UBACYT 20020130100262BA, PICT-2015-2285, PICT 2015-0801, LNLS-Brazil under Proposal (XAFS-2) 20160632. Xunta de Galicia, Spain (ED431C 2017/22) and European Union's H2020 programme INSPIRED-646155.

Appendix A. Supplementary material

Supplementary data associated with this article can be found, in the online version, at https://doi.org/10.1016/j.jcis.2018.01.083.

References

[1] S. Yamazoe, K. Koyasu, T. Tsukuda, Nonscalable oxidation catalysis of gold clusters, Acc. Chem. Res. 47 (2014) 816–824, https://doi.org/10.1021/ar400209a.
[2] N. Vilar-Vidal, J. Rivas, M.A. López-Quintela, Metal(0) Clusters in Catalysis, in: W. Chen, S. Chen (Eds.), Funct. Nanometer-Sized Clust. Transit. Met., Royal Society of Chemistry, Cambridge, 2014: pp. 226–260. doi:10.1039/9781782628514.
[3] A. Corma, P. Concepción, M. Boronat, M.J. Sabater, J. Navas, M.J. Yacaman, E. Larios, A. Posadas, M.A. López-Quintela, D. Buceta, E. Mendoza, G. Guilera, A. Mayoral, Exceptional oxidation activity with size-controlled supported gold clusters of low atomicity, Nat. Chem. 5 (2013) 775–781, https://doi.org/10.1038/nchem.1721.
[4] N. Vilar-Vidal, J.R. Rey, M.A. López, Quintela green emitter copper clusters as highly efficient and reusable visible degradation photocatalysts, Small 10 (2014) 3632–3636, https://doi.org/10.1002/smll.201400679.
[5] C. Deraedt, G. Melaet, W.T. Ralston, R. Ye, G.A. Somorjai, Platinum and other transition metal nanoclusters (Pd, Rh) Stabilized by PAMAM dendrimer as excellent heterogeneous catalysts: application to the methylcyclopentane (MCP) hydrogenative isomerization, Nano Lett. 17 (2017) 1853–1862, https://doi.org/10.1021/acs.nanolett.6b05156.
[6] Y. Chen, C. Zeng, D.R. Kauffman, R. Jin, Tuning the magic size of atomically precise gold nanoclusters via isomeric methylbenzenethiols, Nano Lett. 15 (2015) 3603–3609, https://doi.org/10.1021/acs.nanolett.5b01122.
[7] S. Wang, X. Gao, X. Hang, X. Zhu, H. Han, W. Liao, W. Chen, Ultrafine Pt nanoclusters confined in a calixarene-based Ni24 coordination cage for high-efficient hydrogen evolution reaction, J. Am. Chem. Soc. 138 (2016) 16236–16239, https://doi.org/10.1021/jacs.6b11218.
[8] B. Liu, H. Yao, W. Song, L. Jin, I.M. Mosa, J.F. Rusling, S.L. Suib, J. He, Ligand-free noble metal nanocluster catalysts on carbon supports via "Soft" Nitriding, J. Am. Chem. Soc. 138 (2016) 4718–4721, https://doi.org/10.1021/jacs.6b01702.
[9] Q.-F. Zhang, P.G. Williard, L.-S. Wang, Polymorphism of phosphine-protected gold nanoclusters: synthesis and characterization of a new 22-gold-atom cluster, Small. 12 (2016) 2518–2525, https://doi.org/10.1002/smll.201600407.
[10] S. Srivastava, J.P. Thomas, N. Heinig, M. Abd-Ellah, M.A. Rahman, K.T. Leung, Efficient photoelectrochemical water splitting on ultrasmall defect-rich TaO_x nanoclusters enhanced by size-selected Pt nanocluster promoters, Nanoscale. 9 (2017) 14395–14404, https://doi.org/10.1039/C7NR04378C.
[11] S. Zhuang, L. Liao, M.-B. Li, C. Yao, Y. Zhao, H. Dong, J. Li, H. Deng, L. Li, Z. Wu, The fcc structure isomerization in gold nanoclusters, Nanoscale. 9 (2017) 14809–14813, https://doi.org/10.1039/C7NR05239A.
[12] F. Alonso, P. Riente, J.A. Sirvent, M. Yus, Nickel nanoparticles in hydrogen-transfer reductions: characterisation and nature of the catalyst, Appl. Catal. A Gen. 378 (2010) 42–51, https://doi.org/10.1016/j.apcata.2010.01.044.
[13] J. Oliver-Messeguer, L. Liu, S. García-García, C. Canós-Giménez, I. Domínguez, R. Gavara, A. Doménech-Carbó, P. Concepción, A. Leyva-Pérez, A. Corma, Stabilized naked sub-nanometric cu clusters within a polymeric film catalyze C–N, C–C, C–O, C–S, and C–P Bond-Forming Reactions, J. Am. Chem. Soc. 137 (2015) 3894–3900, https://doi.org/10.1021/jacs.5b00222.
[14] Z. Zhang, X. Wei, Y. Yao, Z. Chen, A. Zhang, W. Li, W.D. Wu, Z. Wu, X.D. Chen, D. Zhao, Conformal coating of Co/N-doped carbon layers into mesoporous silica for highly efficient catalytic dehydrogenation-hydrogenation tandem reactions, Small (2017) 1702243, https://doi.org/10.1002/smll.201702243.
[15] L. Ai, W. Jiang, Z. Liu, J. Liu, Y. Gao, H. Zou, Z. Wu, Z. Wang, Y. Liu, H. Zhang, B. Yang, Engineering a red emission of copper nanocluster self-assembly architectures by employing aromatic thiols as capping ligands, Nanoscale. 9 (2017) 12618–12627, https://doi.org/10.1039/C7NR03985A.
[16] M.F. Calderón, E. Zelaya, G.A. Benitez, P.L. Schilardi, A.H. Creus, A.G. Orive, R.C. Salvarezza, F.J. Ibañez, New findings for the composition and structure of Ni nanoparticles protected with organomercaptan molecules, Langmuir. 29 (2013) 4670–4678, https://doi.org/10.1021/la304993c.
[17] S. Eriksson, U. Nylén, S. Rojas, M. Boutonnet, Preparation of catalysts from microemulsions and their applications in heterogeneous catalysis, Appl. Catal. A Gen. 265 (2004) 207–219, https://doi.org/10.1016/j.apcata.2004.01.014.
[18] A.A. El-Gendy, E.M.M. Ibrahim, V.O. Khavrus, Y. Krupskaya, S. Hampel, A. Leonhardt, B. Büchner, R. Klingeler, The synthesis of carbon coated Fe, Co and Ni nanoparticles and an examination of their magnetic properties, Carbon N. Y. 47 (2009) 2821–2828, https://doi.org/10.1016/j.carbon.2009.06.025.
[19] J.S. Bradley, B. Tesche, W. Busser, M. Maase, M.T. Reetz, Surface Spectroscopic study of the stabilization mechanism for shape-selectively synthesized nanostructured transition metal colloids, J. Am. Chem. Soc. 122 (2000) 4631–4636, https://doi.org/10.1021/ja992409y.
[20] K. Vijayakrishna, K.T.P. Charan, K. Manojkumar, S. Venkatesh, N. Pothanagandhi, A. Sivaramakrishna, P. Mayuri, A.S. Kumar, B. Sreedhar, Ni Nanoparticles stabilized by poly(Ionic Liquids) as chemoselective and magnetically recoverable catalysts for transfer hydrogenation reactions of carbonyl compounds, ChemCatChem. 8 (2016) 1139–1145, https://doi.org/10.1002/cctc.201501313.
[21] M.R. Knecht, J.C. Garcia-Martinez, R.M. Crooks, Synthesis, characterization, and magnetic properties of dendrimer-encapsulated nickel nanoparticles containing <150 Atoms, Chem. Mater. 18 (2006) 5039–5044, https://doi.org/10.1021/cm061272p.
[22] A. Kumar, S. Kang, C. Larriba-Andaluz, H. Ouyang, C.J. Hogan, R.M. Sankaran, Ligand-free Ni nanocluster formation at atmospheric pressure via rapid quenching in a microplasma process, Nanotechnology. 25 (2014) 385601, https://doi.org/10.1088/0957-4484/25/38/385601.
[23] K.S. Joya, L. Sinatra, L.G. AbdulHalim, C.P. Joshi, M.N. Hedhili, O.M. Bakr, I. Hussain, Atomically monodisperse nickel nanoclusters as highly active electrocatalysts for water oxidation, Nanoscale. 8 (2016) 9695–9703, https://doi.org/10.1039/C6NR00709K.
[24] F. Alonso, P. Riente, M. Yus, Nickel nanoparticles in hydrogen transfer reactions, Acc. Chem. Res. 44 (2011) 379–391, https://doi.org/10.1021/ar1001582.
[25] P. Veerakumar, S.-M. Chen, R. Madhu, V. Veeramani, C.-T. Hung, S.-B. Liu, Nickel nanoparticle-decorated porous carbons for highly active catalytic reduction of organic dyes and sensitive detection of Hg(II) Ions, ACS Appl. Mater. Interfaces. 7 (2015) 24810–24821, https://doi.org/10.1021/acsami.5b07900.
[26] C. Wang, J. Tuninetti, Z. Wang, C. Zhang, R. Ciganda, L. Salmon, S. Moya, J. Ruiz, D. Astruc, Hydrolysis of ammonia-borane over Ni/ZIF-8 nanocatalyst: high efficiency, mechanism, and controlled hydrogen release, J. Am. Chem. Soc. 139 (2017) 11610–11615, https://doi.org/10.1021/jacs.7b06859.
[27] N.C. Nelson, T.P.A. Ruberu, M.D. Reichert, J. Vela, Templated synthesis and chemical behavior of nickel nanoparticles within high aspect ratio silica capsules, J. Phys. Chem. C. 117 (2013) 25826–25836, https://doi.org/10.1021/jp409878a.
[28] A.S. Samardak, A.V. Ognev, E.V. Sukovatitsina, M.E. Stebliy, E.B. Modin, L.A. Chebotkevich, R. Mahmoodi, M.G. Hosseini, S.M. Peighambari, F. Nasirpouri, Magnetic behavior of Single Ni nanowires and its arrays embedded in highly ordered nanoporous alumina templates, Solid State Phenom. 215 (2014) 298–305, https://doi.org/10.4028/www.scientific.net/SSP.215.298.
[29] A.S.S. and E.V.S. and A.V.O. and L.A.C. and R.M. and S.M.P. and M.G.H. and F. Nasirpouri, High-density nickel nanowire arrays for data storage applications, J. Phys. Conf. Ser. 345 (2012) 12011. http://stacks.iop.org/1742-6596/345/i=1/a=012011.
[30] A.S. Peinetti, S. Herrera, G.A. Gonzalez, F. Battaglini, Synthesis of atomic metal clusters on nanoporous alumina, Chem. Commun. 49 (2013) 11317–11319, https://doi.org/10.1039/C3CC47170E.
[31] B. Ravel, M. Newville, ATHENA, ARTEMIS, HEPHAESTUS: data analysis for X-ray absorption spectroscopy using IFEFFIT, J. Synchrotron Radiat. 12 (2005) 537–541, https://doi.org/10.1107/S0909049505012719.
[32] K. Nielsch, F. Müller, A.-P. Li, U. Gösele, Uniform nickel deposition into ordered alumina pores by pulsed electrodeposition, Adv. Mater. 12 (2000) 582–586, https://doi.org/10.1002/(SICI)1521-4095(200004)12:8<582::AID-ADMA582>3.0.CO;2-3.

[33] S. Huseyinova, J. Blanco, F.G. Requejo, J.M. Ramallo-López, M.C. Blanco, D. Buceta, M.A. López-Quintela, Synthesis of highly stable surfactant-free Cu5 clusters in water, J. Phys. Chem. C. 120 (2016) 15902–15908, https://doi.org/10.1021/acs.jpcc.5b12227.
[34] Q. Wang, K.H. Lim, S.-W. Yang, Y. Yang, Y. Chen, Atomic carbon adsorption on Ni nanoclusters: a DFT study, Theor. Chem. Acc. 128 (2011) 17–24, https://doi.org/10.1007/s00214-010-0736-4.
[35] P.L. Rodríguez-Kessler, A.R. Rodríguez-Domínguez, Stability of Ni clusters and the adsorption of CH4: first-principles calculations, J. Phys. Chem. C. 119 (2015) 12378–12384, https://doi.org/10.1021/acs.jpcc.5b01738.
[36] M. Walter, J. Akola, O. Lopez-Acevedo, P.D. Jadzinsky, G. Calero, C.J. Ackerson, R.L. Whetten, H. Grönbeck, H. Häkkinen, A unified view of ligand-protected gold clusters as superatom complexes, Proc. Natl. Acad. Sci. 105 (2008) 9157–9162, https://doi.org/10.1073/pnas.0801001105.
[37] G. Sauer, G. Brehm, S. Schneider, K. Nielsch, R.B. Wehrspohn, J. Choi, H. Hofmeister, U. Gösele, Highly ordered monocrystalline silver nanowire arrays, J. Appl. Phys. 91 (2002) 3243–3247.
[38] T. Sehayek, M. Lahav, R. Popovitz-Biro, A. Vaskevich, I. Rubinstein, Template synthesis of nanotubes by room-temperature coalescence of metal nanoparticles, Chem. Mater. 17 (2005) 3743–3748, https://doi.org/10.1021/cm0501057.
[39] E.E. Finney, R.G. Finke, Nanocluster nucleation and growth kinetic and mechanistic studies: a review emphasizing transition-metal nanoclusters, J. Colloid Interface Sci. 317 (2008) 351–374, https://doi.org/10.1016/j.jcis.2007.05.092.
[40] L. Scarabelli, M. Grzelczak, L.M. Liz-Marzán, Tuning gold nanorod synthesis through prereduction with salicylic acid, Chem. Mater. 25 (2013) 4232–4238, https://doi.org/10.1021/cm402177b.
[41] J. Pérez-Juste, I. Pastoriza-Santos, L.M. Liz-Marzán, P. Mulvaney, Gold nanorods: synthesis, characterization and applications, Coord. Chem. Rev. 249 (2005) 1870–1901, https://doi.org/10.1016/j.ccr.2005.01.030.
[42] S.E. Lohse, C.J. Murphy, The quest for shape control: A history of gold nanorod synthesis, Chem. Mater. 25 (2013) 1250–1261, https://doi.org/10.1021/cm303708p.
[43] Y.A. Attia, D. Buceta, C. Blanco-Varela, M.B. Mohamed, G. Barone, M.A. López-Quintela, Structure-directing and high-efficiency photocatalytic hydrogen production by Ag clusters, J. Am. Chem. Soc. 136 (2014) 1182–1185, https://doi.org/10.1021/ja410451m.
[44] Y.A. Attia, C. Vazquez-Vazquez, M.C. Blanco, D. Buceta, M.A. Lopez-Quintela, Gold nanorod synthesis catalysed by Au clusters, Faraday Discuss. 191 (2016) 205–213, https://doi.org/10.1039/C6FD00015K.
[45] N. Vilar-Vidal, J. Rivas, M.A. López-Quintela, Size dependent catalytic activity of reusable subnanometer copper(0) clusters, ACS Catal. 2 (2012) 1693–1697, https://doi.org/10.1021/cs300355n.
[46] A. Fernando, K.L.D.M. Weerawardene, N.V. Karimova, C.M. Aikens, Quantum mechanical studies of large metal, metal oxide, and metal chalcogenide nanoparticles and clusters, Chem. Rev. 115 (2015) 6112–6216, https://doi.org/10.1021/cr500506r.
[47] V. Sharma, K. Park, M. Srinivasarao, Colloidal dispersion of gold nanorods: Historical background, optical properties, seed-mediated synthesis, shape separation and self-assembly, Mater. Sci. Eng. R Reports. 65 (2009) 1–38, https://doi.org/10.1016/j.mser.2009.02.002.
[48] T.R. Kline, M. Tian, J. Wang, A. Sen, M.W.H. Chan, T.E. Mallouk, Template-grown metal nanowires, Inorg. Chem. 45 (2006) 7555–7565, https://doi.org/10.1021/IC0601384.